Journal Pre-proof

Zn supported on Zr modified mesoporous SBA-15 as sorbents of pollutant precursors contained in fossil fuels: Si/Zr ratio effect

J.A. Colín-Luna, G.E. Zamora-Rodea, A.K. Medina-Mendoza, L. Alvarado-Perea, Carlos Angeles-Chávez, J. Escobar, J.G. Pacheco-Sosa, J.C. García Martínez

PII: S0920-5861(19)30585-1

DOI: https://doi.org/10.1016/j.cattod.2019.10.023

Reference: CATTOD 12528

To appear in: *Catalysis Today*

Received Date: 14 April 2019

Revised Date: 29 September 2019

Accepted Date: 12 October 2019

Please cite this article as: Colín-Luna JA, Zamora-Rodea GE, Medina-Mendoza AK, Alvarado-Perea L, Angeles-Chávez C, Escobar J, Pacheco-Sosa JG, García Martínez JC, Zn supported on Zr modified mesoporous SBA-15 as sorbents of pollutant precursors contained in fossil fuels: Si/Zr ratio effect, *Catalysis Today* (2019), doi: https://doi.org/10.1016/j.cattod.2019.10.023

Zn supported on Zr modified mesoporous SBA-15 as sorbents of pollutant precursors contained in fossil fuels: Si/Zr ratio effect

J. A. Colín-Luna[a]*, G. E. Zamora-Rodea[a], A.K. Medina-Mendoza[a], L. Alvarado-Perea[b], Carlos Angeles-Chávez[c], J. Escobar[c], J.G. Pacheco-Sosa[d], J.C. García Martínez[a]

[a]*Universidad Autónoma Metrópolitana-Azcapotzalco, Departamento de Energía, Área de Análisis de Procesos, Av. San Pablo 180, Col. Reynosa, CP. 02200, México, CDMX.*

[b]*Universidad Autónoma de Zacatecas, Unidad Académica de Ciencias Químicas y Maestría en Ciencias de la Ingeniería, Campus UAZ Siglo XXI, Carretera Zacatecas-Guadalajara km 6, Ejido La Escondida, CP. 98160, Zacatecas, México.*

[c]*Instituto Mexicano del Petróleo, Dir. Inv. Transformación de Hidrocarburos, Eje Central Lázaro Cárdenas Norte 152, 07730, CDMX, México.*

[d] *Universidad Juárez Autónoma de Tabasco (UJAT), División Académica de Ciencias Básicas, Km 1, Carretera Cunduacán-Jalpa de Méndez, Col. La Esmeralda, CP. 8669, Cunduacán, Tabasco, México.*

(*) corresponding author: jacl@azc.uam.mx

Graphical abstract

ADSORPTION ISOTHERMS

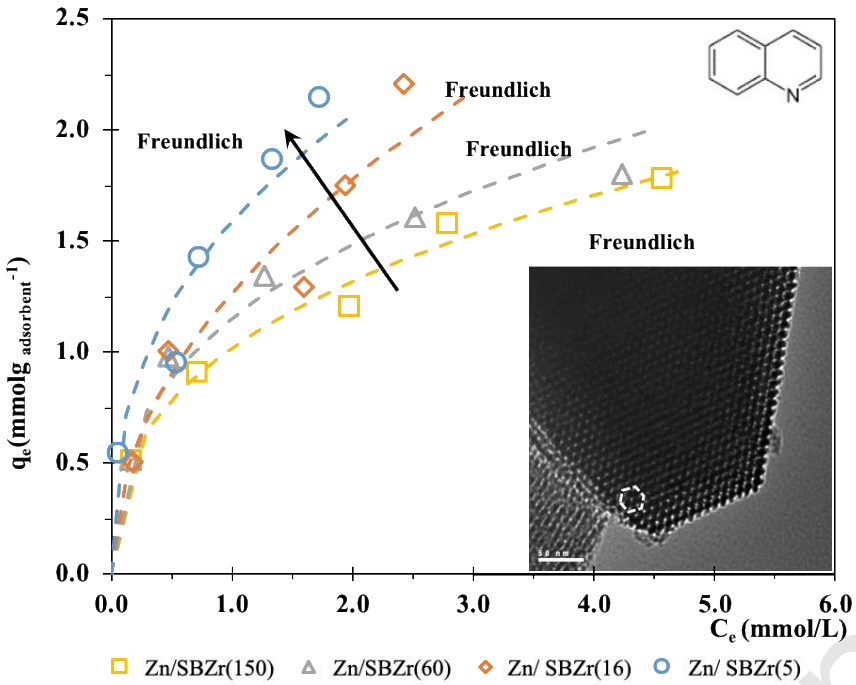

Highlights

- The impregnation of the Zr conserve the arrangement and the textural properties.
- The adsorption capacity of organonitrogen molecules depends on the Si/Zr ratio.
- To adsorb organosulphur molecules is necessary to introduce a metal adsorption site.
- Langmuir or Freundlich isotherms depends on the Si/Zr ratio and the metal site.
- Adsorbents Zn/SBZr(5) can be regenerated without important loss adsorption capacity.

Abstract

The adsption processes have become an additional alternative to hydrotreatment processes of oil-derived middle distillates. The crucial point is the type of adsorbent employed. SBA-15 mesoporous materials were used to adsorb quinoline (Q) and dibenzothiophene (DBT) as N- and S-containing model species, respectively, contained in a model mixture mimicking middle distillates. Q and DBT in dodecane solutions (50-250 ppm and 500 ppm, respectively) were used to that end. In order to improve the adsorption properties, SBA-15 was modified, incorporating

zirconium at Si/Zr weight ratios of 5, 16, 60, and 150. At those ratios, Q was adsorbed preferably, whereas DBT was removed only below 10%. To increase the amount of S adsorbed, Zn was incorporated at 2 wt. %. At 250 ppm (sol. concentration) of N, the amount adsorbed of Q and DBT on the material without Zn (Si/Zr=5) was 1.51 and 0.02 $mmolg_{ads}^{-1}$, respectively. The results were notably different when Zn was incorporated in adsorbents. In these case, amounts of adsorbed Q and DBT were 2.2 and 1.3 $mmolg_{ads}^{-1}$, respectively, showing that metal sites are essential to adsorb DBT.

Keywords: Ultra Low Sulfur Diesel; SBA-15; Adsorption processes; Sustainable processes; Hydrodesulfurization.

1. Introduction

In the last decades, fossil fuels have been the most widely used energy source in the world for almost all industrial and economic activities [1]. However, its combustion generates pollutants such as SO_2 or NO_X, in addition to CO_2. Due to the damage that these products cause, environmental legislation has been strengthened, limiting S content in diesel to less than 5 ppm [1, 2]. To reach these levels, hydrodesulfurization (HDS) offers an immediate solution to produce cleaner fuels [2,3]. However, the effectiveness of the process is dependent on the type of middle distillate to be processed [2,4]. In naphtha feedstocks, the HDS process is highly effective because most of the organo-S species present consist of mercaptans, thiophenes, alkyl thiophene, and benzothiophenes. Benzothiophenes and alkylbenzothiophenes are present in jet fuel [4]. However, in the case of middle-distillates dialkyldibenzothiophenes are present, their reactivity at commercial reaction conditions (623 K and 7 MPa) is very low due to the steric hindrances by the methyl groups adjacent to the S atom [2-5]. On the other hand, the organo-nitrogen species

contained in those middle distillates compete with de organo-sulfur ones by active sites of the catalysts decreasing S removal [6]. The HDS becomes highly expensive due to the necessity of frequent regenerations or loading of fresh catalysts besides H_2 high consumption. Then, to reach the demanded S content targets in fossil fuels, the development of new economic and sustainable processes is enticing. The adsorption of N- and S- bearing species before HDS seems to be convenient due to its low temperature (~320 K) and pressure requirements (up to 0.1 MPa) [2]. In those processes, there is no H_2 consumption, and the adsorbed species can be later desorbed to be used as fertilizer or as raw materials of pharmaceutical products [1]. The critical point is the adsorbent material because it must have textural and physicochemical properties suitable for the adsorption of nitrogen-bearing species and, if possible, also of organo-sulfur ones of the dibenzothiophene type [7-8]. The choice of these materials should be made considering adsorption capacity, selectivity, regenerability, lifetime, and price. In the literature, it has been reported the use of zeolites [9-13], activated carbon [14-19], metal-organic frameworks [20-21], and mesoporous materials like MCM-41 and SBA-15 [22-26]. Due to their acid properties, zeolites are reported as highly sulfur-selective adsorbents. According to Liao et al. [13], the adsorption of benzene or thiophene depends on the type of acid site (Lewis or Brønsted). Nevertheless, in an extensive consensus in the literature, this high capacity and selectivity towards the sulfur compounds are not only due to its acid properties but rather to the incorporation of metals (Cu^{+1}, Ag^{+1}, Fe^{+2}, Zn^{+2}, Cd^{+2}, Mn^{+2} or Ni^{+2}) in the cavities of the zeolite [11-13]. Ahmad et al. [27] found that the incorporation of Zn in clays improved the adsorption of S. However, the narrow pore diameter (1.26 nm) did not allow higher adsorption of organo-S species. Some drawbacks restrict their use in industrial processes. Although they have surface areas close to 200 m^2/g, the narrow pore size (< 2 nm) of the microporous order could prevent the

adsorption of large species such as dialkyldibenzothiophenes contained in middle distillates fractions.

One possibility to remove sulfur compounds of larger size is employing mesoporous silica-based materials [22-23, 26-31] with pores size larger than 3 nm and surface areas nearby 1000 m^2/g. Recently, our group probes several types of mesoporous materials such as SBA-15, SBA-16, and MCM-41 as adsorbents of DBT and Q (as model species representing those in middle distillates) at 318 K and atmospheric pressure in a batch system [24, 25]. It was found that high surface area and Si-OH groups (Brønsted acid sites) allowed selective adsorption of Q but weak retention of the sulfur-bearing species. It was shown that suitable pore size is essential for Q removal but not in the case of DBT [25].

In the search for new, more selective adsorbent materials with a large capacity to remove highly polluting organic compounds, SBA-15 constitutes materials of high potential to be used as adsorbents of organo-nitrogen and organo-sulfur compounds. Therefore, in the present work, Zr over SBA-15 matrix modified at several Si/Zr ratios were investigated to adsorb organo-N and organo-S compounds. Also, a metal site (Zn) was studied as S adsorption center in a model mixture containing DBT, Q, and dodecane (DOD) as a solvent. Finally, as an approximation to the use of those materials at industrial conditions, several adsorption-regeneration cycles were carried out to determine the feasibility of materials reused.

2. Experimental

2.1. Synthesis of SBA-15 and the Zr-modified materials

In a typical preparation essay, 16 g of Pluronic P123 ($EO_{20}PO_{70}EO_{20}$, from Sigma-Aldrich) was dissolved in 474 ml of 2 M HCl solution and 26 ml water with stirring at 298 K until dissolution of the structuring agent. Then 32 g of TEOS was added into that solution with stirring at 311 K

for 24 h. The mixture was aged at 368 K for 72 h without stirring. The solid obtained was filtered and washed with abundant deionized water. Finally, the solid SBA-15 was calcined at 823 K for 6 h, with a 0.8 K min^{-1} heating rate to remove the structuring agent and unclog the pores [32]. Zirconium was introduced into the SBA-15 via post-synthetic method by a grafting procedure to obtain Zr-modified SBA-15 [33]. Zirconium (IV) isopropoxide ($Zr(C_3H_7O)_4$) at 70 wt.% solution in 1-propanol) was used as the zirconium source, and absolute ethanol (EtOH) was used as solvent (99.999%). A fraction of calcined SBA-15 was slurried in EtOH containing $Zr(iso\text{-}PrO)_4$ for 8 h at room temperature. In order to eliminate excess $Zr(iso\text{-}PrO)_4$, the filtered material was washed with anhydrous EtOH. The solid was then dried in air at room temperature and calcined in airflow at 823 K for 5 h. The ratio SiO_2/ZrO_2 in wt% was equal to 5, 16, 60, and 150. Materials were identified by using the key: SBZr(X) where X stands for the Si/Zr mass ratio in the solid.

2.2. SBZr(X) impregnated with Zn synthesis

Zinc was incorporated into SBZr support by a solid-state impregnation (SSI) method [34]. A finely ground powder fraction of the SiZr was dried in static air to 393 K for 12 h; then, it was directly mixed with the precursor zinc salt (zinc nitrate, Aldrich 98%) to have a 2 wt% nominal content of Zn in the final solid. The mixture was mechanically ground in an agate mortar for 0.5 h. Finally, the material was thermally treated in a dynamic inert atmosphere at 823 K for 6 h and at 10 K min^{-1} heating rate. Hereinafter materials will be identified by the key Zn/SBZr(X) where X stands for the Si/Zr mass ratio in the solid.

2.3 Materials characterization

2.3.1. X-ray diffraction

X-ray powder diffraction patterns were recorded on a Bruker D8 diffractometer using a monochromatized CuK_α radiation (λ = 0.154 nm) in 5 to 70 ° range for XRD at high angle and from 0.5 to 7 ° range for XRD at small angle, both at 2θ scale, with scanning rate of 0.01° (2θ)/s.

2.3.2 Nitrogen physisorption

Nitrogen physisorption measurements were carried out at 77 K on an ASAP 2010 Micromeritics apparatus. The isotherms were used to quantify the textural properties of the samples. The specific surface areas (S_{BET}) of the samples were calculated using the BET method in the standard pressure range of 0.05 - 0.3 P/P_0. The total pore volume (V_P) was evaluated based on the amount adsorbed at a relative pressure of about 0.98, by converting the amount of nitrogen gas adsorbed at STP to the liquid volume at 77 K (using the conversion factor c = 0.001547). The pore size (d_P) were obtained from the desorption branch of the isotherm using the corrected form of the Kelvin equation using the Barrett–Joyner–Halenda method with a cylindrical pore model [35].

2.3.3. FTIR analysis

FTIR spectra of Zn/SBZr(X) pure solids adsorbents were obtained in the mid-infrared range (4000 – 400 cm^{-1}) using a Perkin-Elmer IR spectrophotometer model Spectrum One with an Attenuated Total Reflectance (ATR) accessory. To gain more information about the adsorption of sulfur (DBT) and nitrogen molecules (Q) on the adsorbents surface, used SBA and Zn/SBZr(16) were analyzed as a representatives samples after the adsorption process. As described in detail below, the samples were treated during 3 h with a mixture to dodecane (DOD), Q (250 ppm of N) and DBT (500 ppm). After that, these samples were filtered and dried at room temperature during 24 h. For both kind of samples: pure solids and used, the spectra were collected in transmission mode employing 50 scans at a spectral resolution of 4 cm^{-1} at room temperature. Prior to the

measurement of each soil sample, the FTIR-ATR crystal was cleaned, and background spectra were obtained for subsequent baseline correction.

2.3.4 Transmission electron microscopy

Chemical and morphological characterizations were performed by HR-TEM (JEM-2200FS transmission electron microscope operated at 200 kV). The elemental chemical analysis was performed by EDX spectroscopy with EDAX and NORAN spectrometers attached to the microscopes, Nova Nano Lab Dual Beam, and JEM-2200FS, respectively. The samples were ground, suspended in isopropanol at room temperature, and dispersed with ultrasonic agitation. Some drops of solutions were put onto a lacey carbon copper grid (3 mm in diameter).

2.3.5. Adsorption tests

The adsorption tests were carried out at 313 K and 78 kPa in jacketed glass containers. To each vessel was added 40 mL of DOD with Q and DBT as the nitrogen (N) and sulfur (S) containing species, respectively, at concentrations of 50 - 250 ppm of N with 500 ppm of S and 0.2 g of adsorbent under vigorous stirring. Finally, the samples were analyzed by a gas chromatograph equipped with capillary column and FID. During the first hour, samples were collected every 10 minutes and then every 15 minutes during the next two hours. Liquid was filtered, and then samples were injected to the gas chromatograph as reported in previous works [24, 25].

The adsorption capacity of each adsorbent was determined through the adsorption maximum that is, the equilibrium concentration. Therefore, the amount of adsorbed component respecting the amount of adsorbent was obtained using the eqn. (1):

$$q_e = \frac{(C_0 - C_e)V}{m} \tag{1}$$

Where q_e is the maximum adsorbed amount ($mmolg_{adsorbent}^{-1}$); V is the volume of adsorbed the substance (adsorbate, in L); m is the mass of the adsorbent material (in g); C_0 and C_e are the adsorbates initial and equilibrium concentrations expressed in mmol L^{-1}.

To gain better understanding of the adsorption process, kinetic and isotherm models were used to fit the experimental data. A second-order kinetic model was tested in its differential and linear form [36], eqns. (2) and (3), respectively.

$$\frac{dq}{dt} = k(q_e - q)^2 \tag{2}$$

$$\frac{t}{q} = \frac{1}{k\,q_e^2} + \frac{t}{q_e} \tag{3}$$

Where q is the amount adsorbed per unit of adsorbent ($mmolg_{adsorbent}^{-1}$); t is the adsorption time (min), and k is the adsorption kinetic constant ($g_{adsorbent}$ $mmol^{-1}min^{-1}$).

The experimental data were fitted to Langmuir and Freundlinch isotherms; these expressions are given by eqns. (4) and (5):

$$q_e = \frac{q_m K_L C_e}{1 + K_L C_e} \tag{4}$$

$$q_e = K_F C_e^{1/n} \tag{5}$$

Where q_m is the adsorption maximum (in $mmolg_{adsorbent}^{-1}$), K_L (in $Lmmol^{-1}$) and K_F (in $mmolg_{adsorbent}^{-1}L^{1/n}mmol^{-1/n}$) are the Langmuir and Freundlich constants, respectively, C_e is the equilibrium concentration (in $mmolL^{-1}$), and q_e is the maximum adsorbed amount ($mmolg_{adsorbent}^{-}$

[1]). According to Shahriar et al. [31], *1/n* represents the adsorption capacity, depending on nature and strength of adsorption and indicates the relative energy sites distribution. K_F is the adsorption capacity. The larger K_F and smaller *1/n* the more effective could be the adsorbent. K_L, K_F, and q_m were experimentally obtained by plotting the linear form of Langmuir and Freundlich eqns., (6) and (7), respectively:

$$\frac{C_e}{q_e} = \frac{1}{q_m K_L} + \frac{C_e}{q_m} \quad (6)$$

$$ln\, q = ln\, K_F + \frac{1}{n} C_e \quad (7)$$

2.3.5. Regeneration tests

Regeneration tests were performed for the material of higher adsorption capacity. Thus, the material used in the first adsorption test was recovered, washed with 30 mL of acetone maintaining constant stirring, then filtered, allowed to dry at room temperature during 12 h, then dried in an oven at 368 K for 12 h being finally calcined at 823 K for 6 h. The regenerated material was tested in the adsorption of Q at 250 ppm and 500 ppm of S under the conditions described in section 2.3.5. The regeneration procedure was thrice performed.

3. Results and discussion

3.1 Structural analysis by XRD at low and wide-angle

Figure 1 shows small-angle diffraction patterns of the SBA-15 material and those modified with Zr. The characteristic peaks of the SBA-15 (Figure 1a) could be identified at 0.9, 1.4 and 1.8 of 2θ values corresponding to (100), (110) and (200) respectively, diffraction planes with d(100) spacing of around 11 nm. According to these results, SBA-15 shows a highly ordered two-dimensional hexagonal mesoporous structure (*p6mm*) characteristic of those materials, suggesting an excellent long-range order within the material [37-40]. Diffraction patterns of SBA-15 at different Si/Zr ratios are shown in Figures 1b-1e. It can be seen that the three characteristic peaks of hexagonal arrange are maintained, decreasing in intensity as the Zr content in solids increases. This behavior was also observed by incorporating the zinc in the SBZr(X) materials (Figure 2). These results indicated decreased hexagonal porous array when Zr and Zn were incorporated to the SBA-15 [37]. Wide-angle diffraction patterns of Zn/SBZr(X) are shown in Figure 3. Just the typical basal reflections of amorphous silica were observed at around 24°. No diffraction peaks corresponding to ZnO and ZrO_2 phases were observed indicating that metal phases were well dispersed into/over the SBA-15 matrix as amorphous phases or nanocrystals which size was below the XRD detection limit (> 5 nm).

Nitrogen adsorption-desorption isotherms for SBZr(X) and Zn/SBZr(5) are shown in Figure 4. According to the classification of the International Union of Pure and Applied Chemistry (IUPAC) [35], those isotherms are type IV with H1 hysteresis loop between 0.6 and 0.75 of relative pressure. According to the literature [39, 40], this behavior is characteristic of capillary condensation in cylindrical mesopores of open ends, characteristic of SBA-15 materials. Textural properties of mesoporous adsorbents are given in Table 1. Initially, SBA -15 had S_{BET} as high as 665 m^2g^{-1} with V_P of 1.02 cm^3g^{-1} and d_P of 5.7 nm, values of the order of those previously reported in the literature for similar solids [37-40]. For SBA modified with Zr, a variation of surface area with zirconium content could be observed. In particular, at high Zr contents, SBZr(5)

presents a decrease of 10% in that parameter. However, at lower Zr content S_{BET} increases according to the order SBZr(16) < SBZr(60) < SBZr(150). That behavior could be attributed to ZrO_2 domains formed on the SBA-15 surface increasing the specific area at Si/Zr ratios above 16, while at Si/Zr ratios below 5 the S_{BET} tends to diminish due to non-porous ZrO_2 agglomerates formation. In terms of d_P and V_P, no significant changes by Zr addition were observed.

Zn/SBZr(5) sample was chosen to investigate the textural properties of materials loaded with Zn. This solid had around 10% decreased textural properties (S_{BET}, d_P, and V_P) as to SBZr(X) materials. Unit cell parameter (a_0) remained nearly constant in all materials, Table 1. The slight changes observed were congruent with those found by XRD. Similar behavior was registered regarding wall thickness (E_P) that was practically constant with an average value of 7 nm, suggesting that prepared solids were mechanically and hydrothermally stable.

3.2 FTIR spectra

Infrared spectra for different synthesized materials are shown in Figure 5. The characteristic bands of SiO_4 vibrations were located between 500 and 1200 cm^{-1}. Si-O-Si bonds vibration could be observed at 1082 cm^{-1} due to asymmetric stretching and at 797 cm^{-1}, while bands at 1600 and 3500 cm^{-1} corresponded to O-H type bonds, which were attributed to the presence of water and surface and bridged hydroxyl groups, respectively. The band at 1628 cm^{-1} corresponded to O-H vibrations of silanol groups. Finally, the absorption at 975 cm^{-1} was assigned to the stretch mode of [SiO_4] linked to heteroatoms. Thus, Zn linked to SBZr(X) surface was evidenced [37, 41].

For the samples used and non-used, Figure 6 shows FTIR-ATR spectra in order to investigate the Q and DBT molecules adsorption mechanism on the adsorbents. In Figures 6a and 6b non-used SBA and Zn/SiZr(16) spectra are shown, respectively. As mentioned above, characteristic vibrational stretching of Si-O-Si, silanol groups and [SiO_4] interacting with the metal oxides were observed in these materials. Regarding the adsorbents used, Zn/SBZr(16) and SBA spectra

(Figures 6c and 6d), appeared bands corresponding to the solvent and sulfur (DBT) and nitrogen (Q) organocompounds. For these spectra, is noteworthy that the band at 3350 cm^{-1} does not appear indicating an interaction of DBT with hydroxyl groups via H-bonding as have been reported in other works [42-44]. Nevertheless, these OH groups are protonic sites able to react with basic molecules as Q. In Figure 6c and 6d three intensive bands were detected in the region 2760 to 3020 cm^{-1}. According to literature [42, 44] these bands corresponding to aliphatic methyl (CH_3-, 2960 cm^{-1}), methylene groups (-CH_2-, 2920 cm^{-1} and 2851 cm^{-1}). On these spectra two minor peaks can be observed at 1450 and 1380 cm^{-1}, the first is associated to -CH_2- groups and second band to C=N groups [45] corresponding to Q adsorbed on metal oxide. The next intensive and broad band at 1050 cm^{-1} is assigned to mixed oxides as was mentioned in Figure 5. The intensity and broad of this band in Figure 6c can be associated to interactions of both molecules DBT and Q with the Zn and Si-O-Si groups in contrast to the low intensity and broad of this peak in Figure 6d. In both spectra of used Zn/SBZr(16) and SBA (Figure 6c and 6d) two peaks are appreciated at 805 and 780 cm^{-1} this peaks also can be associated to DBT and Q with the mixed oxides. The low intensity of these peaks in Figure 6d suggests an effect of Zn in the adsorption of the hetero-compounds. Finally, in both Figure 6c and 6d, it can be observed a shoulder at 740 cm^{-1} and a thin band at 719 cm^{-1}, these peaks are associated to H_2C-S-CH_2 and chain hydrocarbons groups of type -$(CH_2)_n$- [42]. According to Nazal et al. [42-43] these peaks indicate that DBT lies flat on the surface of these materials. Until our knowledge, the adsorption form in these materials is not well established, these results could clarify the adsorption mechanism on these materials.

3.3 HRTEM and elementary chemical analysis by EDX

Figures 7a) to d) showed the morphology of Zn/SBZr(X) solids characterized by their typical mesoporous array. In Fig. 7a) and 7b) it could be observed a longitudinal section of the channels of the pores (samples Zn/SBZr(5) and Zn/SBZr(16)). From those micrographs, the corresponding

pore size was ~5 nm, whereas wall thicknesses were around 6 nm, values close to those reported in Table 1. From Figure 7c) corresponding to Zn/SBZr(60) sample, a cross-section showing the hexagonal array of pores characteristic of this material could be observed, which is in full agreement with that observed from XRD (Figure 2). Figure 7d) shows the quasi-tubular morphology of Zn/SBZr(150). According to those images, incorporating Zn did not modify the hexagonal porous array during the grafting and impregnation steps. Besides, at studied magnifications, neither ZrO_2 nor ZnO defined particles were observed suggesting Zr and Zn domains were very small (<5 nm) and therefore were well distributed in the SBA channels, as also inferred by XRD.

Elementary chemical analyses were carried out by EDX on the Zn/SBZr(X) solids; Table 2 shows the metal contents (Zr and Zn) on SBA-15 matrices expressed in weight and atomic percent bases. As expected, O and Si species exhibited an average weight content of 49.2 (65.4 at%) and 43.0 (32.5 at%), respectively. Although Zn-modified solids were prepared at nominal 2 wt % loading, the estimated average content in all materials was 3.22 wt% (1.06 at%). The clearest difference was found in the Zn/SBZr(60) solid, which had 1.6 wt.%(0.5 at.%) of Zn, 20% lower value than the nominal content. Zn/SBZr(5) and Zn/SBZr(16) had Zr average content of 9% (2.2 at%). Through the results mentioned above, can be calculated the atomic ratio Zr/Si and Zn/Si to determine the metallic dispersion of Zr and Zn on the SBA. As can be observed in Figure 8, the order of dispersion percentage of Zr goes in the order Zn/SBZr(5) ~ Zn/SBZr(16) >> Zn/SBZr(60) > Zn/SBZr(150). As was expected, these results indicate that Zr atoms are well dispersed of the SBA to low Si/Zr ratios. As for the Zn atoms, the Zn/Si atomic ratios go to the order Zn/SBZr(10) > Zn/SBZr(5) ~ Zn/SBZr(60) >> Zn/SBZr(150). In this case, a slight difference occurs between Zn/SiZr(5) and Zn/SiZr(10) in dispersion values, suggesting a good

dispersion of Zn on SBA. At high Si/Zr ratios low dispersion values of Zn/SBZr(60) and Zn/SBZr(150) suggest a decrease in Zn atom number exposed.

3.4 Adsorption tests

3.4.1 Nitrogen and sulfur compounds removal

Removal of N and S compounds employing SBZr(X) and Zn/SBZr(X) at Q contents of 50, 100, 200 y 250 ppm of N as Q and 500 ppm of S as DBT are shown in Figure 9(A) to (D). According to Figure 9(A), the N removal is greater than 90% for materials at Si /Zr ratios of 5 and 60 in the entire range of N concentrations tested. In the opposite, for SBZr(150) and SBZr(16), the amount of N compounds removed was always less than 90%. For pristine SBA-15 and corresponding Zr-modified solid at SBZr(5) similar Q removal capacity was observed when tested in presence of solutions at 50 ppm Q content. From these results, it could be noticed that the cation contributes to improving the ability of adsorption of modified materials. Although the SBZr(5) and SBZr(60) formulations had decreased adsorption capacity when increasing the N content in testing solutions that effect was lower than that observed for SBZr(16) and SBZr(150) which suggested an influence of the amount of incorporated Zr. S species adsorption from solutions at various N concentrations tested was always below 15% SBZr(X) for all studied materials. S adsorption followed the order SBZr(5) >> SBZr(60)> SBZr(150) > SBZr(16). From these results, minimal differences in adsorption capacity throughout the range of N concentrations were observed for SBZr(60) and SBZr(150). Only in the case of the SBZr(16) sample enhanced S adsorption was observed by increasing N content in testing solutions. However, that was not greater than 6%. In Figures 8(C) and 9(D) significant differences could be observed regarding adsorption capacity of various Zn modified formulations as those previously registered for solids prepared with no zinc. According to Figure 9(C), the N adsorption was above 90% at low Q contents while at concentrations above 200 ppm Q the amount removed was higher than 70% for all tested solids.

The order of adsorption capability for N compounds was Zn/SBZr(5) >> Zn/SBZr(16)> Zn/SBZr(60)> Zn/SBZr(150). From Figure 9(D), the amount of S adsorbed was much higher as to those observed for adsorbents without Zn. The highest amounts removed was found at low N contents (50 ppm). The amount of S removed over various tested materials followed the order Zn/SBZr(5) ≈ Zn/SBZr(16) > Zn/SBZr(60)> Zn/SBZr(150). By using the Zn/SBZr(X) adsorbents, it could be possible to remove both heteroatoms at amounts above 80%, a percentage higher than that previously reported by our working group [24, 25].

To get a better understanding of the adsorption process on these adsorbents, kinetic analysis, and adsorption studies were carried out on SBZr(X) and Zn/SBZr(X) solids. However, due to the large number of corresponding results, just those obtained by using one of the best adsorbents are discussed in the following. Thus, Zn/SBZr(5) had removal percentages of N and S compounds above 90% and 80%, respectively.

3.4.2 Kinetic analysis

Adsorption kinetics was investigated correlating experimental data to a pseudo-second-order kinetics (eqn. 3). Figure 10 shows the DBT removal (500 ppm initial concentration) profiles from solutions at various N concentrations (0-250 ppm) respecting time. Employing Zn/SBZr(5) the highest adsorption amount was reached with solutions at 250 ppm, whereas the lowest was found for the corresponding one at 100 ppm. The results of experimental data fitting to eqn. (3) are shown in Tables 3 to 5. Adsorption constants for Q and DBT using SBZr(X) are favored at low N contents and high Zr loadings (Table 3), as discussed in section 3.4.1. From eqn. (3) q_e is another critical parameter to determine the behavior of the adsorption rate. Utilizing SBZr(X) solids the q_e values with Q are much larger than those of DBT. For example, over SBZr(5) at 200 ppm N, the q_e is one order of magnitude larger using Q as to that of DBT (2.05 and 0.24 $mmolg^{-1}$,

respectively), in agreement with the observed removal percentage (Figures 9(A) and 9(B)). DBT adsorption was enhanced when Zn is incorporated to tested materials. For the same adsorbent at 200 ppm N, the value of Q and S adsorbed per gram of adsorbent were 1.87 and 1.4 $mmolg^{-1}$, respectively. Q adsorption increases with the Zr loading. Zn could be an S adsorption site (compare Figures 9(B) and 9(D). q_e for both Q and DBT over Zn/SBZr(X) decreased with the Zr loading, but the decreased was much more pronounced for the S species suggesting that different adsorption sites were involved in each case.

3.4.3 Adsorption analysis

Figures 11 and 12 show experimental results of adsorption to the equilibrium q_e versus C_e for Q (in presence of 500 ppm S) using various SBZr(X) adsorbents with and without Zn, respectively. The dashed lines indicate the fitting of experimental data to equations (4) and (5), Langmuir and Freundlich models, respectively. For SBZr(X) adsorbents at higher Zr content, the experimental data were well fitted by Langmuir isotherms (eqn. 6) while for the SBZr(150) solid the Freundlich isotherm was more suitable (eqn.7). The linear form of the Langmuir isotherm given by the eqn. (6) provided K_L and q_m values of 2.2 $Lmmol^{-1}$ and 3.2 $mmolg^{-1}$, respectively, with a 0.988 correlation coefficient. For SBZr(150) K_F and $1/n$ were 1.02, and 0.7, respectively, with a 0.976 correlation coefficient. According to the literature [31], that adsorbent may be suitable for Q adsorption as compared to other adsorbents that followed the Freundlich model. For Zn-containing adsorbents, the experimental data were better fitted by Freundlich isotherm irrespective of Zr loading in various tested materials. Determined K_F and $1/n$ values and corresponding correlation coefficients (R^2) as well are shown in Table 6. The highest K_F $(1/n)^{-1}$ ratio was found for the Zn/SBZr(5) adsorbent. According to the literature [31], the most effective adsorbent could be the one with the highest K_F and smallest ($1/n$). Therefore, the Zn/SBZr(5) material constituted a very promising adsorbent to remove both nitrogen and sulfur compounds.

3.4.3 Regenerations tests

Table 7 shows adsorption results of Q and DBT (at 250 and 500 ppm, respectively) using the Zn/SBZr(5) solid, as the best of our adsorbents, after various regeneration cycles. Amounts of adsorbed Q and DBT per gram of adsorbent (q_e) did not decrease by more than 50% after the first adsorption. However, according to k_{ads} values, the adsorption process could be significantly slower. A similar reduction was also found in the % removal. This result is not surprising because during the washing and regeneration steps adsorbent mass loss in unavoidable. There could also be loss of porous order (causing diminished textural properties) accompanied by decreased number of adsorption sites due to metal leaching. However, after the first regeneration cycle mentioned, adsorption parameters remained rather constant, suggesting that tested materials could be used in several subsequent adsorption cycles with no substantially different behavior. Therefore, these results show that at high loadings of nitrogen (250 ppm) and sulfur (500 ppm) compounds after the first use, the adsorption properties: q_e, $k_{ads,}$ and removal % remain unchanged.

Rui et al. [10] employed Zn on zeolites to remove sulfur compounds in model molecules mimicking those from naphtha; they found removal percentages between 50 to 80 after four adsorption cycles. However, the metal loading used were between 4 to 8 wt%, almost four times higher than Zn used in the present paper. Besides, as a model mixture, those authors used thiophene alone as sulfur source diluted in cyclohexane (representing then model naphtha), different to other works [21, 23, 25] that used dibenzothiophene or dialquildibenzothiophene and nitrogen compounds as quinoline dissolved in dodecane (corresponding to model middle-distillates). Thaligari et al. [15, 18] demonstrated that when using Zn adsorbents on granular activated carbon, the removal % of the organo-sulfur molecule after the first treatment was reduced to 95%. In their experiments, they used DBT dissolved in n-octadecane in the absence of

nitrogen compounds. Those works claimed the regenerability of the adsorbents but in conditions of less competition for the adsorption sites [10, 15, 18] or, as in the case of Thaligari et al. [18], to a single regenerability test. In our opinion, the present paper shows a complete work on textural and physicochemical properties of our modified SBA-15 materials modulated in the adsorption of organo-nitrogen and -sulfur species at contents similar to those found in oil-derived middle distillates [46].

As final comments, it should be noted that the results clearly show a high adsorption capacity and regenerability of SBA materials modified with Zr. But additionally, the results found in this work would allow deducing a mechanism of the adsorption of the sulfur and nitrogen compounds. It is evident that the Q is well adsorbed when the Zr is present, as could be observed in the case of adsorbents at Si/Zr 5 and 16 ratios. This may be because the cation zirconium is replacing silicon atoms creating an imbalance of charges that generate acidic sites conducive to the basic molecule. The nature and type of acidity have been widely reported in the literature [47]. Therefore, acid sites are sites of adsorption of Q. As can be observed in section 3.3, the high dispersion of Zr allows to suppose that Q preferentially is adsorbed in these acid sites. Also FTIR spectra of Figure 6c and 6d are indicating interactions of the mixed oxides with the nitrogen compound. It is not the same in the case of DBT. It was demonstrated that SBA alone (see section 3.4, Figure 9) could not adsorb this sulfur compound; therefore, a function metallic is necessary. FTIR spectra (Figures 6c and 6d) show interactions with the metal oxides via H bonding in according to adsorption results, it seems that both metals are necessary. Nevertheless, the basic molecule will be preferentially adsorbed on the acid sites generated by the Zr, so the sulfur compound will have to compete for those sites in addition to the Zn (see Figures 9c and 9d), also FTIR show this behavior. Therefore, it can propose that the adsorption on DBT preferentially occurs on Zn in flat

positions as discussed in section 3.2. In according to above a schematic model is shown in Figure 13.

4. Conclusions

Zn/SBZr(X) adsorbents with surface area higher than 400 m^2g^{-1} and pore diameters close to 6 nm were obtained. XRD and HRTEM showed that structure and morphological properties of a porous hexagonal array were preserved in materials at Si/Zr wt. ratios of 5, 16, 60, and 150. Wide-angle XRD patterns did not show characteristic peaks of Zn phases, indicating that small particles were well dispersed on the SBA-15 surface. Those results agreed with HRTEM findings. The introduction of zirconium at Si/Zr ratio of 5 and 16 allowed the adsorption of organo-nitrogen species (Q) in lower proportion (<10%) as to that of sulfur species (DBT). It was determined that the adsorption capacity of Q is greater than 90%, and that is affected by the cation (Zr^{4+}) content. However, despite improved properties in nitrogen compound adsorption, zinc addition was not beneficial regarding sulfur compounds retention. Therefore, it was shown that introducing another metal as S adsorption site was necessary. Our results confirmed that this adsorption capacity could be close to 80% for both sulfur and nitrogen compounds and that this property depended on the materials Si/Zr ratio. This ability to remove such heteroatoms was attributed to the high dispersion of Zn with small particle size (<5 nm). Through adsorption kinetic tests, it was shown that adsorption could be very fast, causing immediate saturation of adsorption sites. Adsorption tests at equilibrium suggested that the type of adsorption depends on both Zr and Zn content. At high Zr content, the experimental data followed a Langmuir type model. Conversely, after incorporating Zn, the adsorption at equilibrium followed a Freundlich type model, independently of the Zr loading in adsorbents. Finally, it was demonstrated that after four regeneration cycles the adsorption capacity of prepared materials was still adequate since Q

removal of more than 30% was achieved while for DBT the removal was over 20% higher than values previously found in the literature.

Acknowledgments

G. E. Zamora-Rodea is very grateful to CONACYT for the grant to support his postgrad studies.

References

[1] A. Samokhvalov, B. J. Tatarchuk, Catal Reviews, 52(3)(2010) 381-410.

[2] E. Ito, J.A. Rob van Veen. Catal. Today 116 (2006) 446-460.

[3] H. Wang, R. Prins, J. of Catal 264 (2009) 31-43.

[4] A. Stanislaus, A. Marafi, M. S. Rana, Catal. Today 153 (2010) 1–68.

[5] M. S. Rana, V. Sámano, J. Ancheyta, J.A.I. Diaz, Fuel 86 (2007) 1216–1231.

[6] H. Farag, M. Kishida, H. Al-Megren, Appl. Catal. A: Gen. 469 (2014) 173.

[7] A. Samokhvalov, B. J. Tatarchuk, Catal. Reviews: Sci. and Eng., 52(2010) 381–410.

[8] G.C. Laredo, P. M. Vega-Merino, F. Trejo-Zárraga , J. Castillo, Fuel Process. Tech. 106 (2013) 21–32.

[9] S. Velu, Ch. Song, M. H. Engelhard, Ya-Huei Chin, Ind. Eng. Chem. Res. 44(2005) 5740-5749.

[10] J. Rui, F. Liu, R. Wang, Y. Lu, X. Yang, Molecules 22(2017), 305-317.

[11] Y. Zua, Y. Qina, X. Gaoc, H. Liuc, X. Zhanga, J. Zhanga, L. Song, Appl. Catal. B: Env. 203 (2017) 96–107.

[12] Z.Y. Zhang, T.B. Shi, C.Z. Jia, W.J. Ji, Y. Chen, M.Y. He, Appl. Catal. B: Env. 82 (2008) 1–10.

[13] J. Liao, Y. Zhang, L. Fan, L. Chang, W. Bao, Ind. Eng. Chem. Res. 10.1021/acs.iecr.8b05046.

[14] T.A. Saleh, K.O. Sulaiman, S.A. AL-Hammadi, H. Dafalla, G.I. Danmaliki, J. of Clean. Prod. 154 (2017) 401-412.

[15] S.K. Thaligari, V. Ch. Srivastava, B. Prasad, Clean Tech. Env. Policy 18(2016) 1021–1030.

[16] D. Rameshraja, V. Ch. Srivastava, J. P. Kushwaha, I. D. Mall, Chem. Eng. J. 181– 182 (2012) 343– 351.

[17] J. A. Arcibar-Orozco, J. R. Rangel-Mendez, Chem. Eng. J. 230 (2013) 439–446.

[18] S. K. Thaligari, S. Gupta, V. Ch. Srivastava, B. Prasad, Indian J. of Ch. Tech. 25(2018) 522-530.

[19] S. Jin, Q. Yue, T. Meng, H. Zhang, N. Jiang, M. Jin,·R. Zhang, J Porous Mater 24 (2017)1697–1704.

[20] I. Ahmed, S. H. Jhung, J. of Hazardous Materials 301 (2016) 259-276.

[21] G.C. Laredo, P. M. Vega-Merino, J. A. Montoya-de la Fuente, R. J. Mora-Vallejo, E. Meneses-Ruiz, J. J. Castillo, B. Zapata-Rendón, Fuel 180 (2016) 284–291.

[22] Y. Shi, G. Liu, X. Zhang, Ind. Eng. Chem. Res. 2017, 56, 2557-2564.

[23] S. Shahriar, X. Han, H. Lin, Y. Zheng, Int. J. Chem. React. Eng. 14(4) (2016) 823-830, DOI 10.1515/ijcre-2015-0107.

[24] J.C. García-Martínez, H.A. González Uribe, M.M. González-Brambila, J.A. Colín-Luna, Y.E. Escobedo-García, A. López-Gaona, L. Alvarado-Perea, Catalysis Today 305(2018) 40.

[25] J.C. García-Martínez, C.R. Tapia Medina, M.M. González-Brambila, A.K. Medina-Mendoza, J.A. Colín-Luna, Int. J. of Chem. React. Eng. 2018; 20170238.

[26] J. H. Kim, X. Ma, A. Zhou, Ch. Song, Catalysis Today 111 (2006) 74–83.

[27] W. Ahmad, I. Ahmad, M. Ishaq, K. Ihsan, Arabian J. of Chem. 10 (2014) S3263.

[28] J. M. Palomino, D. T. Tran, J. L. Hauser, H. Dong, S.R.J. Oliver, J. Mater. Chem. A. 2(2014) 14890-14895.

[29] J.L. Hauser, D. T. Tran, E. T. Conley, J. M. Saunders, K. C. Bustillo, S. R. J. Oliver, Chem. Mater. 28(2016) 474−479.

[30] J. You, H. Song, J. Zhang, Ch. Chen, F. Han, Fuel 241 (2019) 997–1007.

[31] S. A. Shahriar, H. Lin, Y. Zheng, Ind. Eng. Chem. Res. 51(2012) 14503−14510.

[32] D. Zhao, Q. Huo, J. Feng, F. Chmelka, G. Stucky, J. of the Am. Chem. Society 120(1998), 6024-6036.

[33] Z. Yongzhong, S. Jaenicke, G. Chuah, J. of Catalysis 218(2003), 396-404.

[34] A.K. Medina-Mendoza, M.A. Cortés-Jácome, J.A. Toledo-Antonio, C. Angeles-Chávez, E. López-Salinas, I. Cuauhtémoc-López, M.C. Barrera, J. Escobar, J. Navarrete, I. Hernández, Appl. Catal. B: Env. 106 (2011), 14-25.

[35] M. Thommes, K. Kaneko, A. V. Neimark, J. P. Olivier, F. Rodriguez-Reinoso, J. Rouquerol, K. S. W. Sing, Pure Appl. Chem.; 87(2015) 9-10, 1051–1069.

[36] S. Azizian, R. N. Fallah, Appl. Surf. Sci. 256 (2010) 5153–5156.

[37] P.H.K. Charan and G. R. Rao, J. Chem. Sci. 127(5)(2015) 909–919.

[38] G. D. Mihai, V. Meynen, M. Mertens, N. Bilba, P. Cool, E. F. Vansant. J. of Materials Sci. 45(2010) 21, 5786–5794.

[39] M. Mureddu, I. Ferino, A. Musinu, A. Ardu, E. Rombi, M. G. Cutrufello, P. Deiana, M. Fantauzzi, C. Cannas. J. of Mater. Chem. A. 45(2014) 19396-19406.

[40] V.Chaudhary, S. Sharma, J Porous Mater (2016) 10.1007/s10934-016-0311-z.

[41] H. Chen, H.Yang, Y. Xi, Micropor. and Mesopor. Mat. 279(2019), 53-60.

[42] M.K. Nazal, M. Khaleda, I.H. Aljundi, M. Atieh, G.A. Oweimreen, A.M. Abulkibash. Env. Tech. 38(2017)23, 2949–2963.

[43] J.Zhang, W.Yin, H.Shang, Ch. Liu. J. of Natural Gas Chem. 17(2008)165–170.

[44] M.A. Larrubia, A. Gutiérrez-Alejandre, J. Ramírez, G. Busca. Appl. Catal. A: Gen. 224 (2002) 167–178.

[45] X.N. Pham, H.Van Doan. Chem. Eng. Comm. 206(2019)9, 1139–1151.

[46] A. Stanislaus, A. Marafi, M. S. Rana, Catal. Today 153 (2010) 1–68.

[47] M.V. Zakharova, F. Kleitz, F.G. Fontaine. Dalton Trans., 46(2017) 3864–3876.

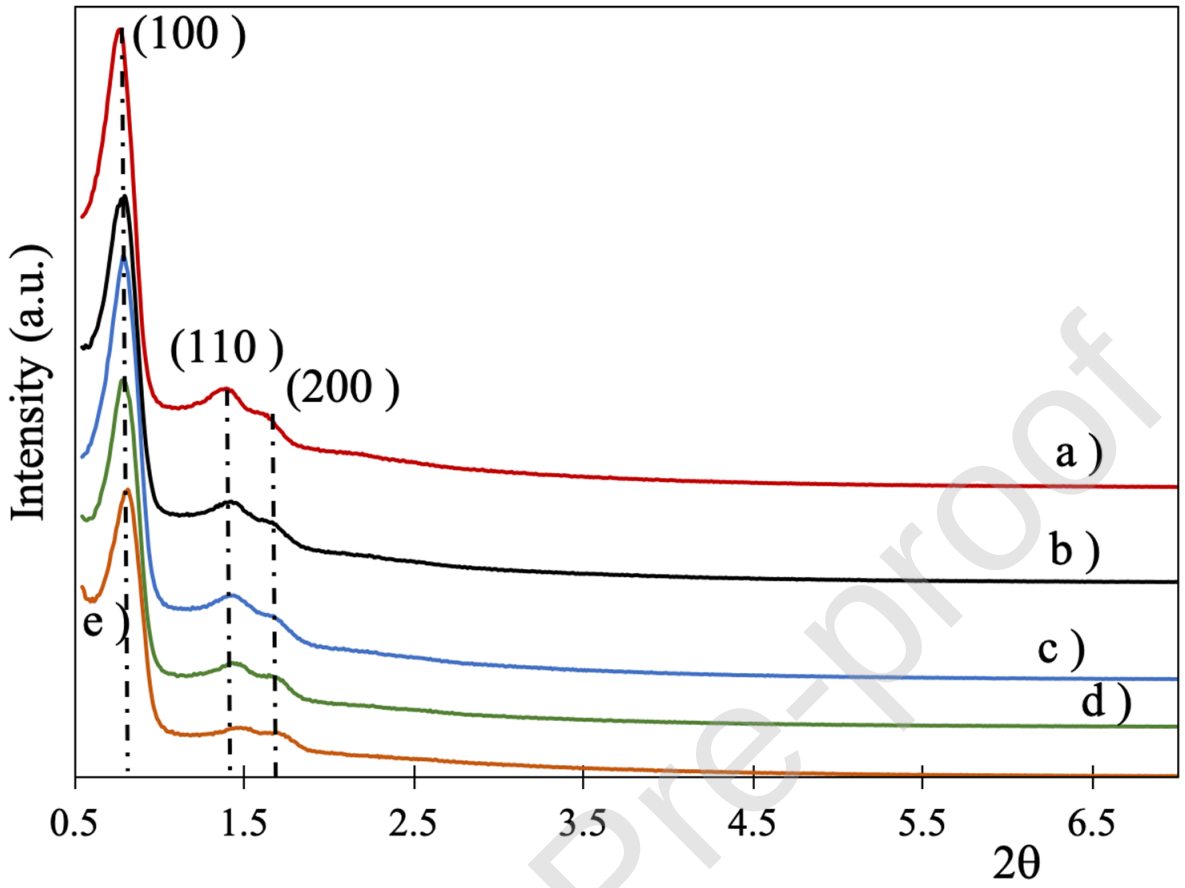

Figure 1. Small-angle XRD patterns of SBA-15 and those modified with Zr: a) SBA, b) SBZr(150), c) SBZr(60), d) SBZr(16) and e) SBZr(5).

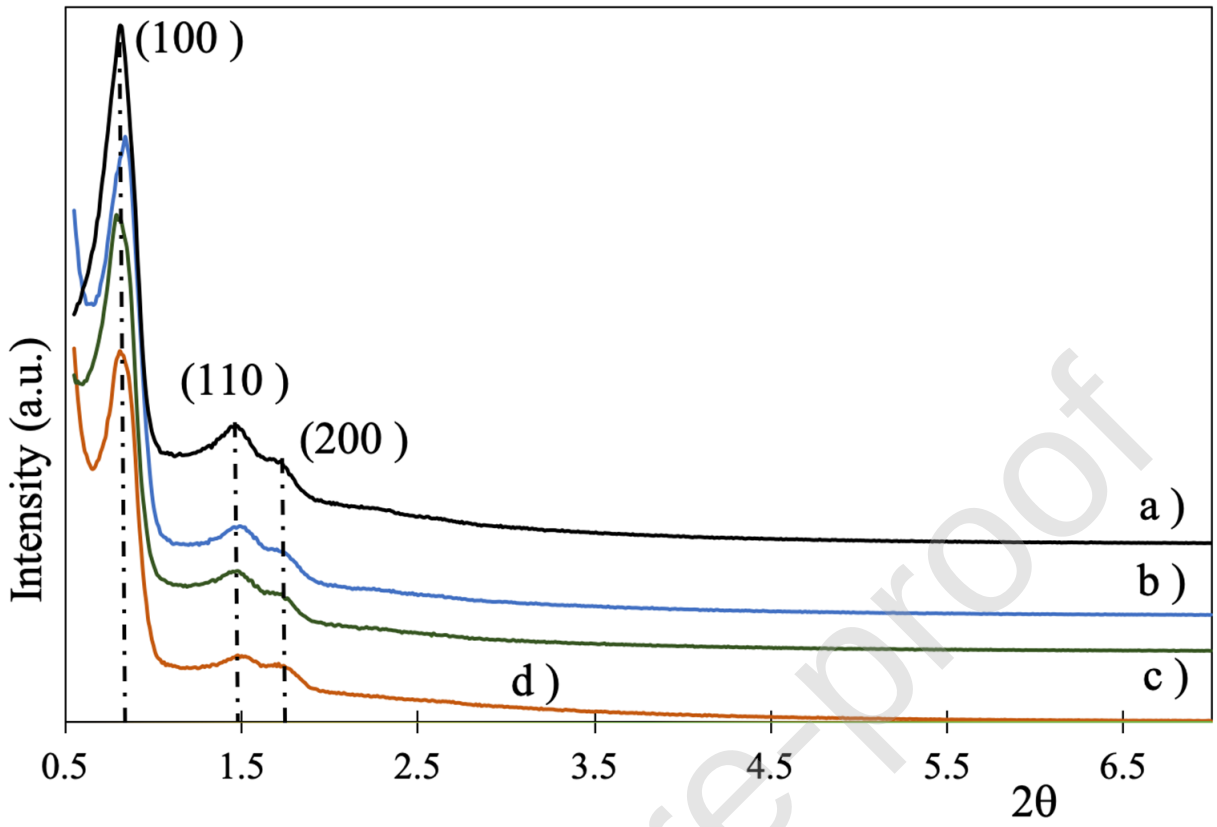

Figure 2. Small-angle XRD patterns of Zn/SBZr(X): a) Zn/SBZr(150), b) Zn/SBZr(60), c) Zn/SBZr(16), d) Zn/SBZr(5).

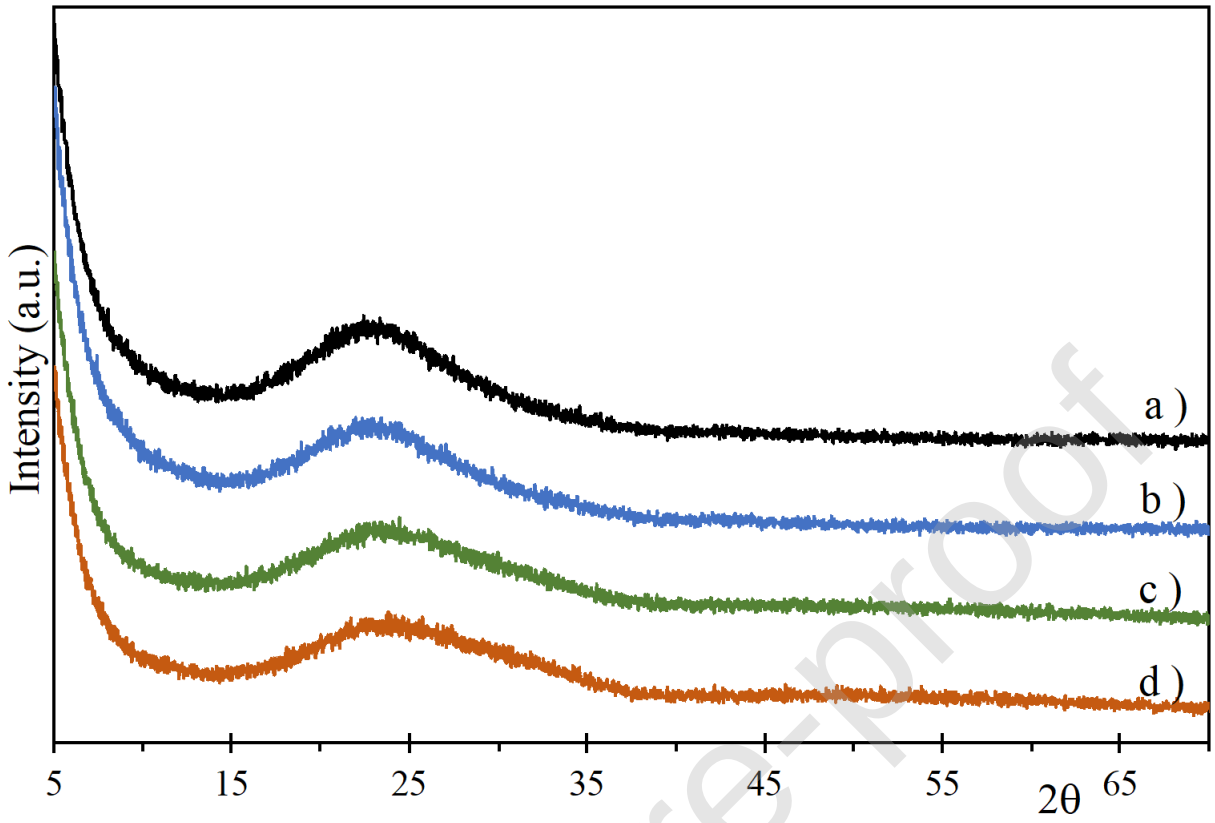

Figure 3. Wide-angle XRD patterns of Zn/SBZr(X): a) Zn/SBZr(150), b) Zn/SBZr(60), c) Zn/SBZr(16), d) Zn/SBZr(5).

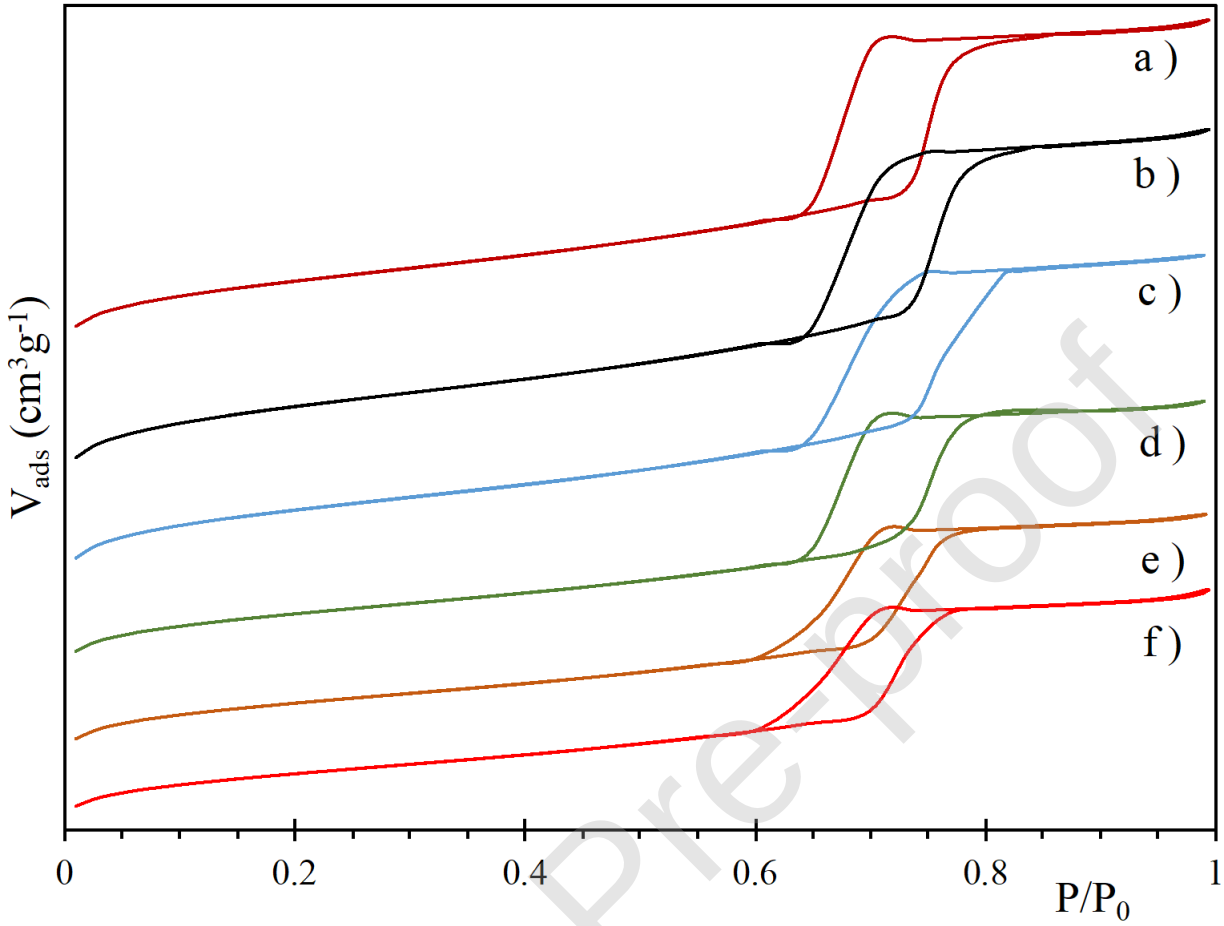

Figure 4. Physisorption isotherms of: a) SBA, b) SBZr(150), c) SBZr(60), d) SBZr(16), e) SBZr(5), f) Zn/SBZr(5).

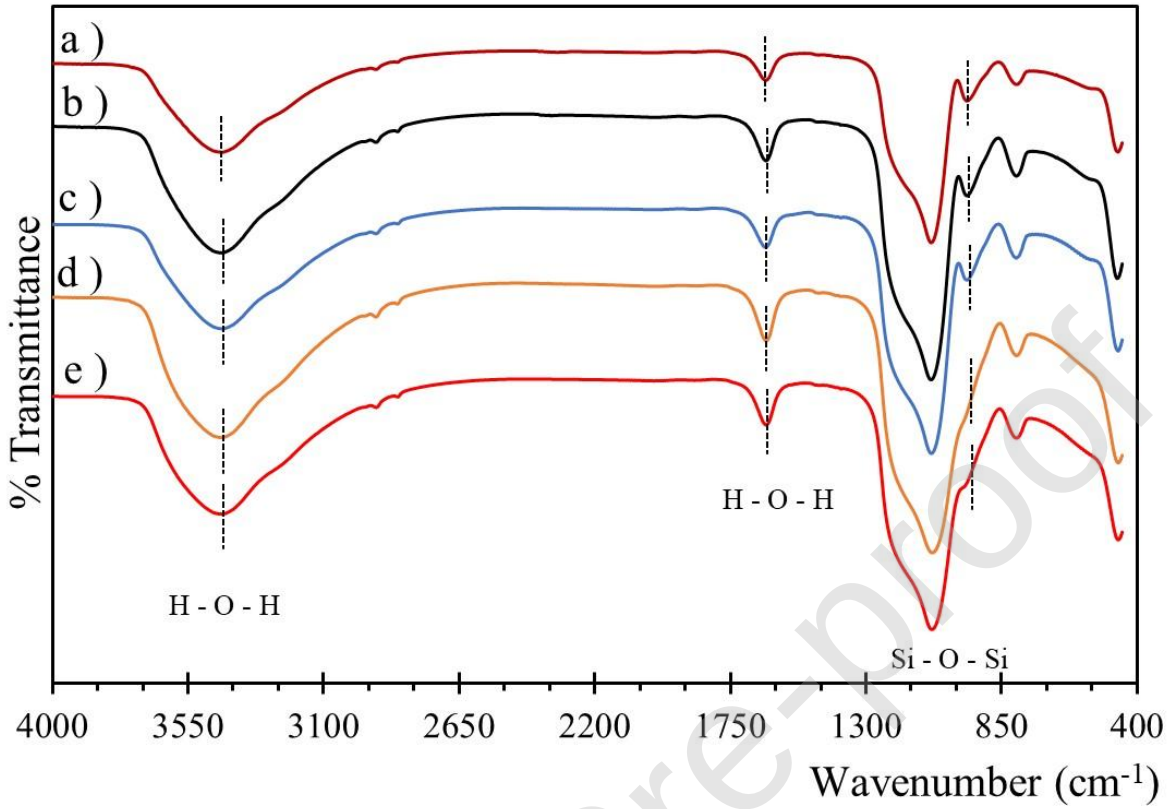

Figure 5. FTIR-ATR spectra of a) SBA, b) Zn/SBZr(150), c) Zn/SBZr(60), d) Zn/SBZr(16), e) Zn/SBZr(5).

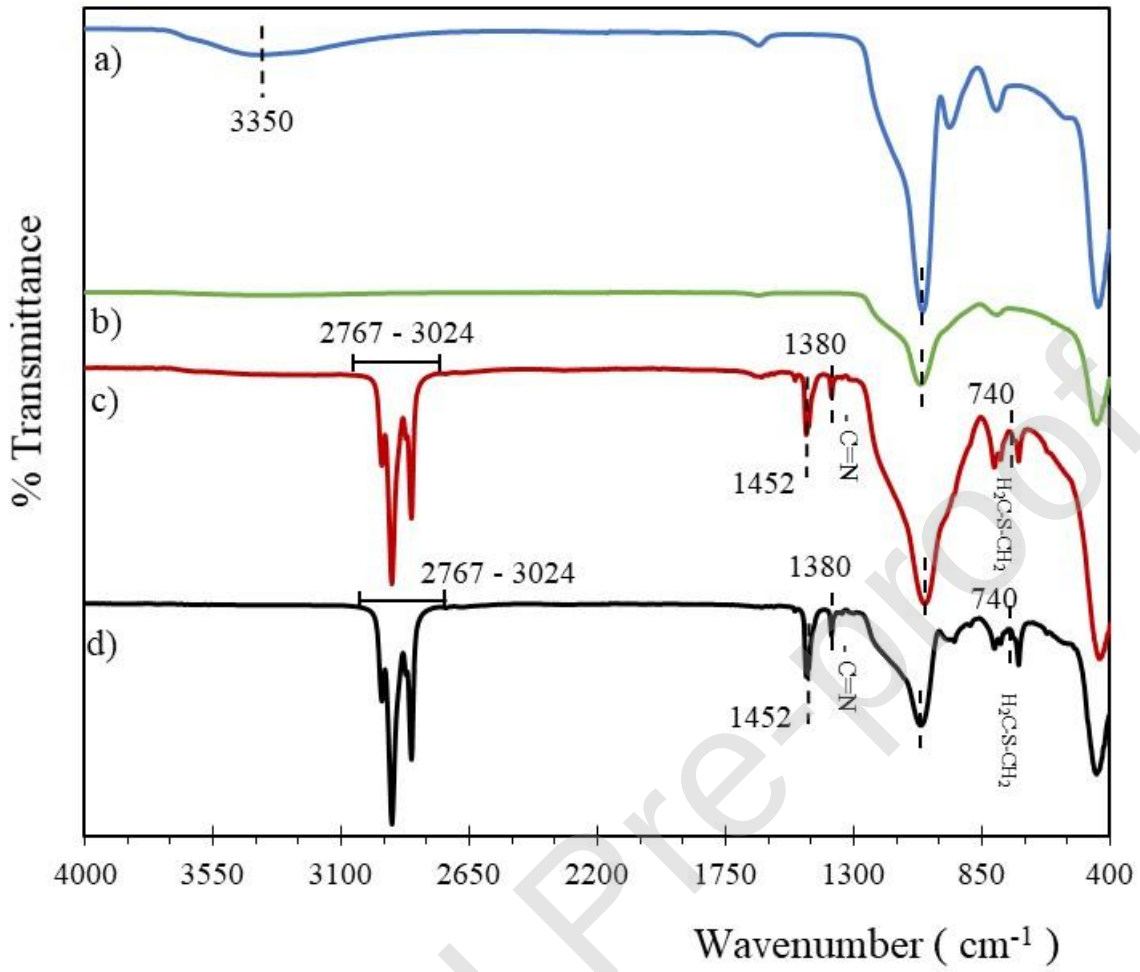

Figure 6. FTIR-ATR spectra of non-used: a) SBA, b) Zn/SBZr(16) and used: c) Zn/SBZr(16), d) SBA.

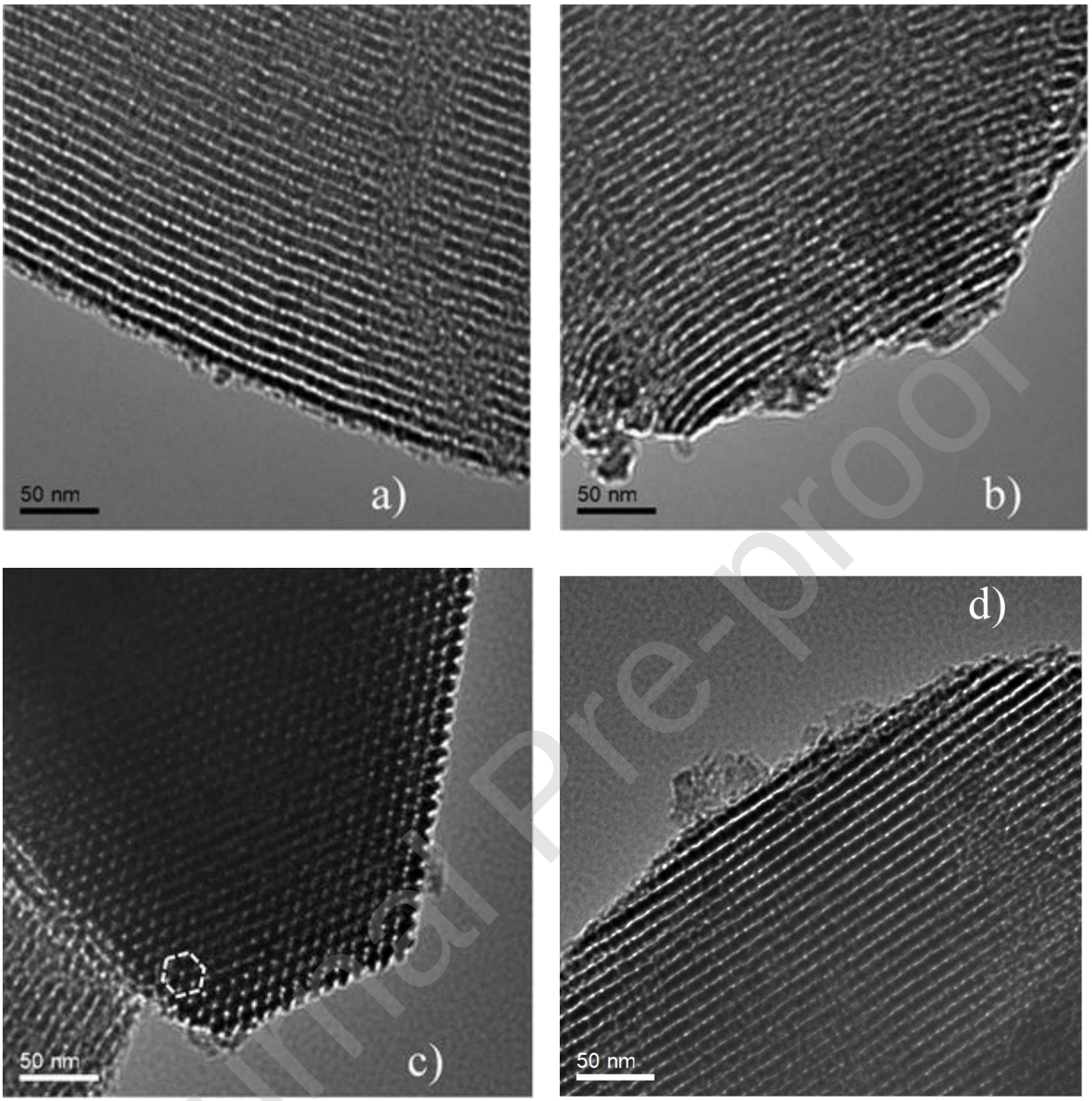

Figure 7. HRTEM images of a) Zn/SBZr(5), b) Zn/SBZr(16), c) Zn/SBZr(60), d) Zn/SBZr(150) as sorbents of Q and DBT as N and sulfur compound, respectively.

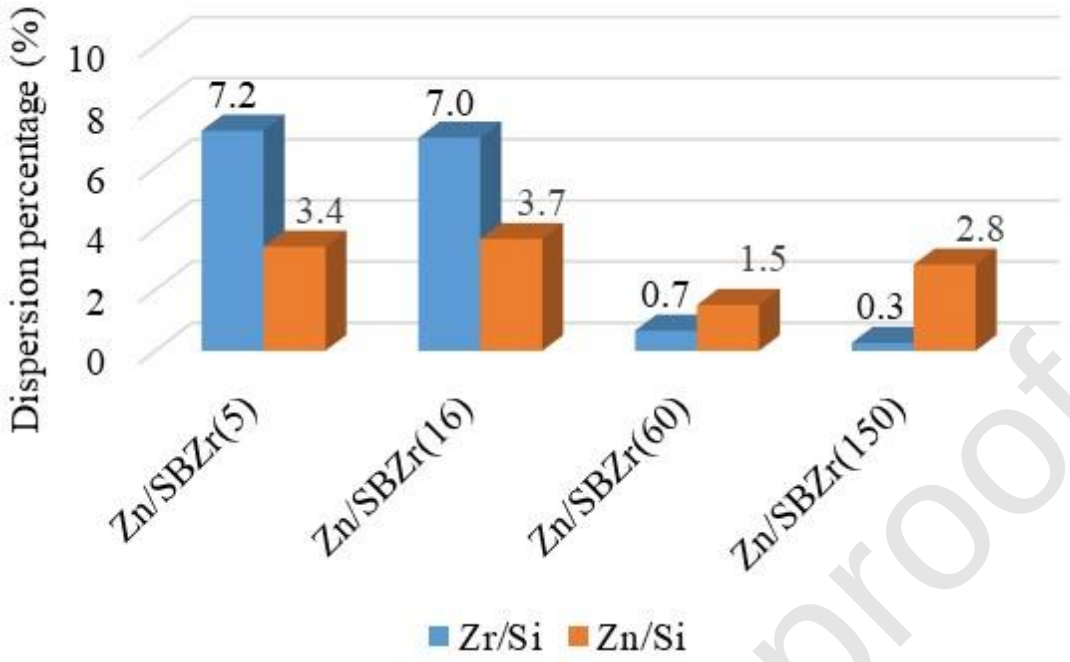

Figure 8. Atomic ratios as a dispersion percentage of Zr and Zn on SBA.

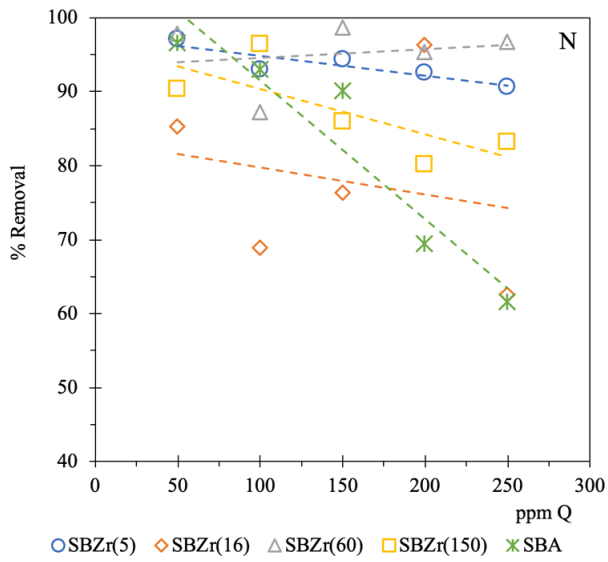

(A)

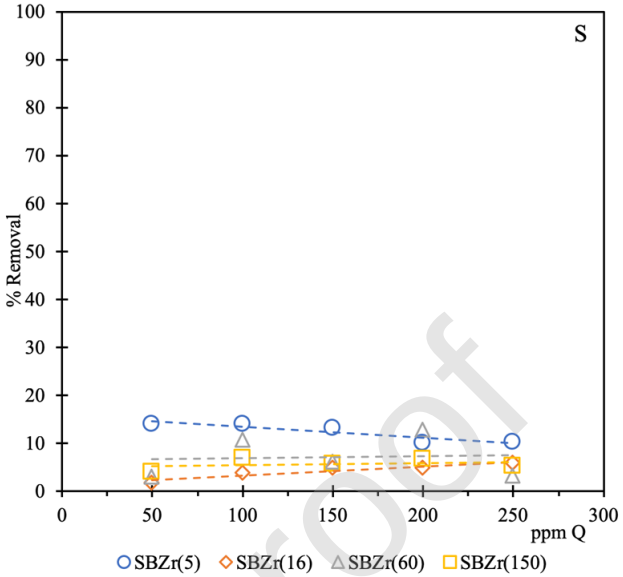

(B)

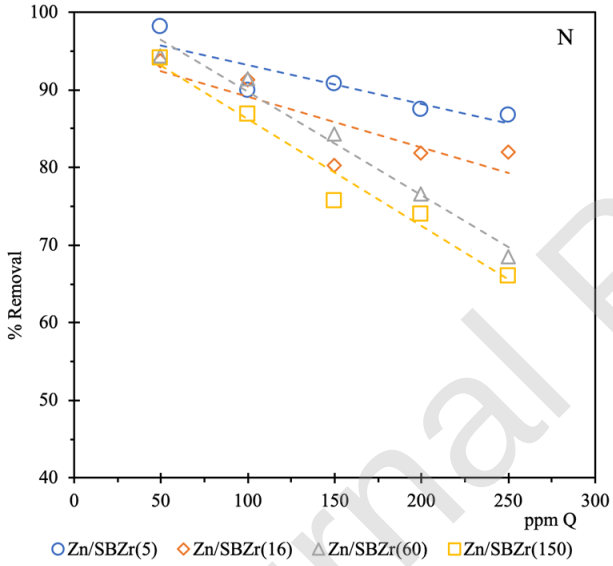

(C)

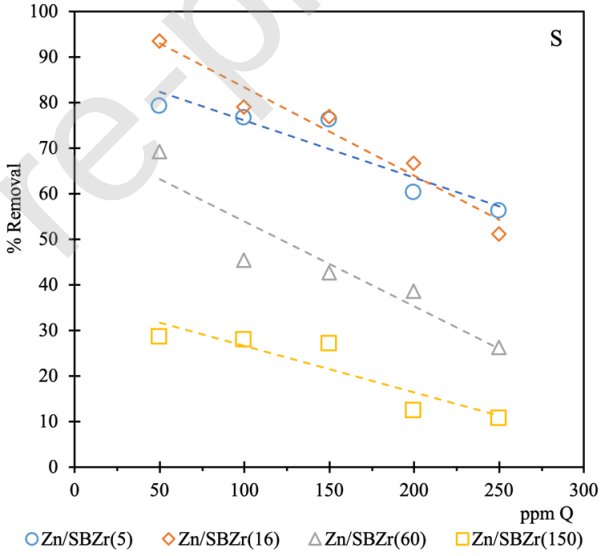

(D)

Figure 9. The percentage removal of nitrogen (N) and sulfur (S) compounds using SBZr(X) (A and B) and Zn/SBZr(X) (C and D), respectively, at several contents of Q and 500 ppm of DBT.

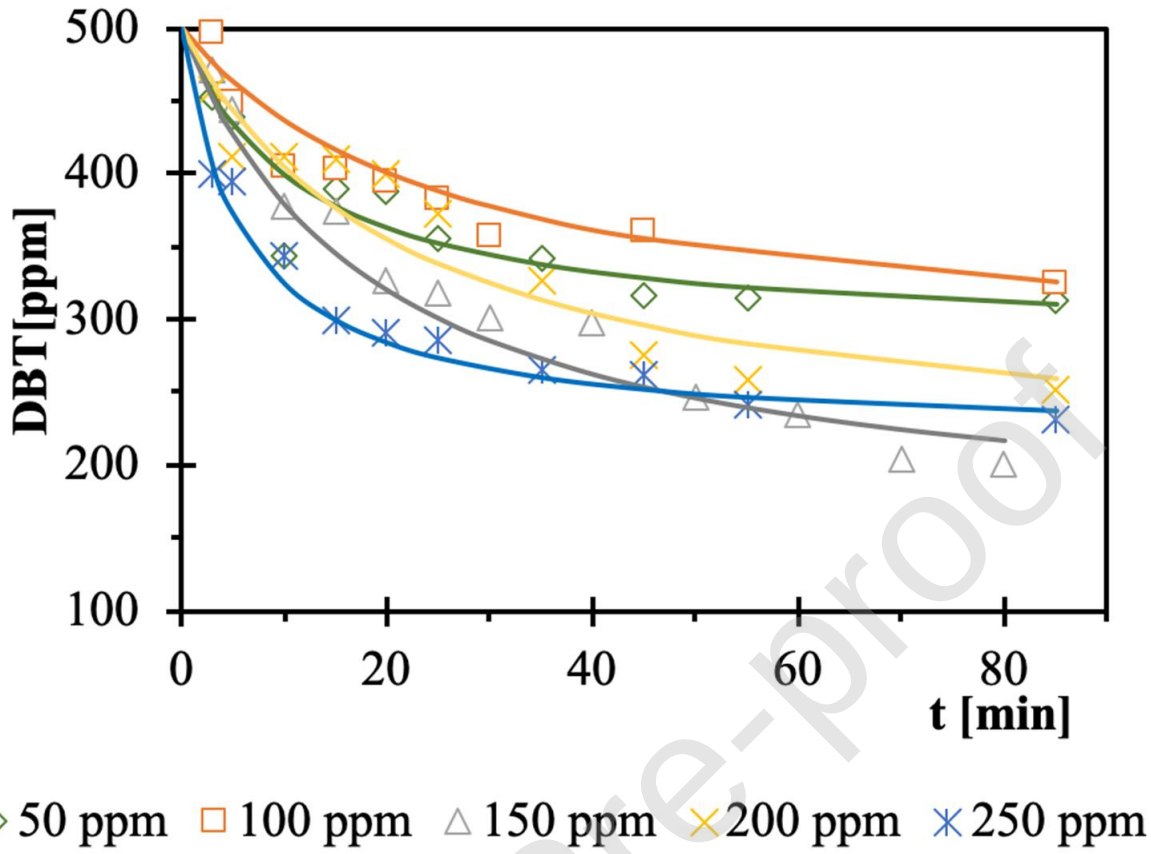

Figure 10. Profile of the Adsorption rate of DBT employing Zn/SBZr(5).

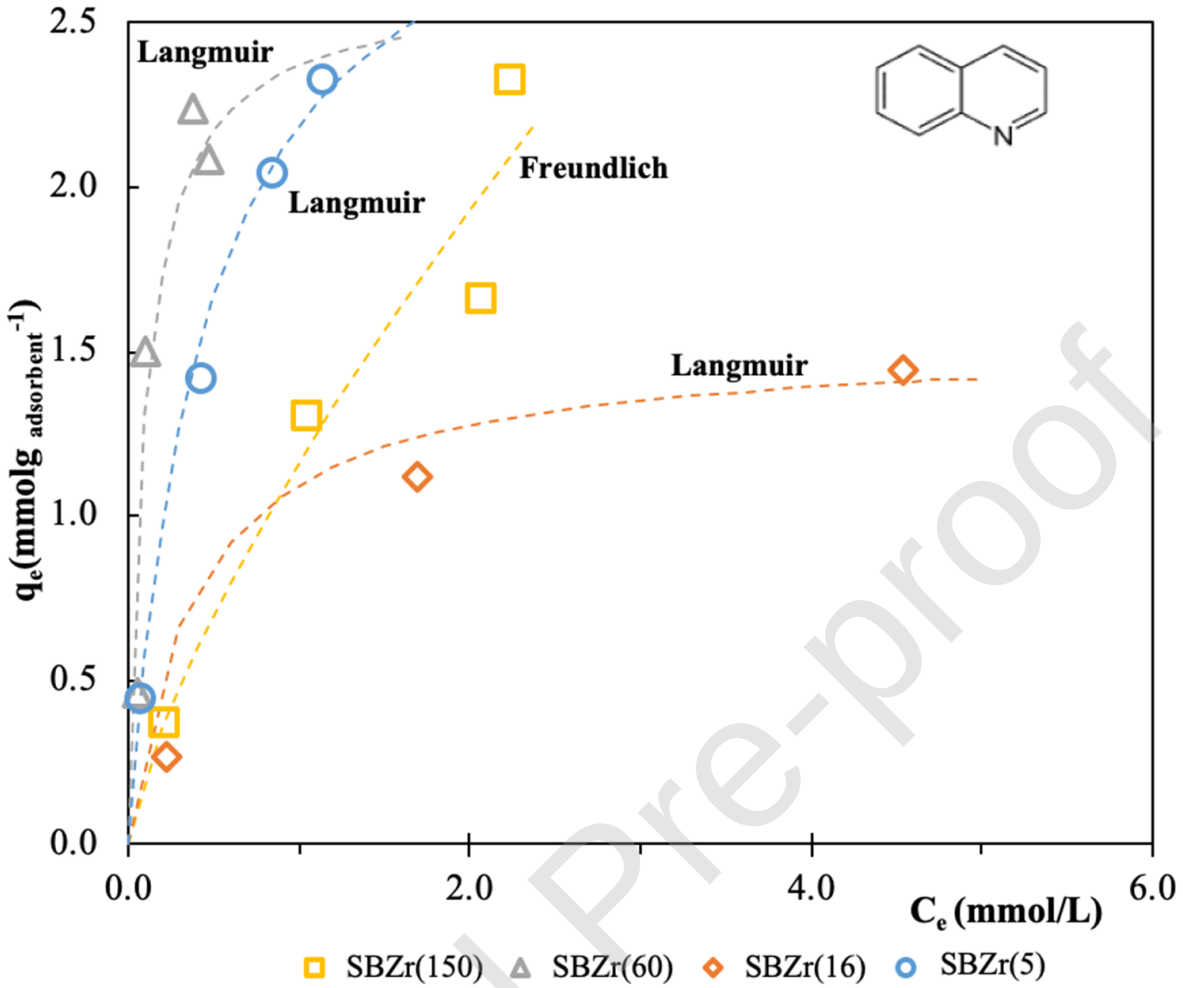

Figure 11. Adsorption isotherms of Q on SBZr(X). Fitted to experimental data in dashed lines.

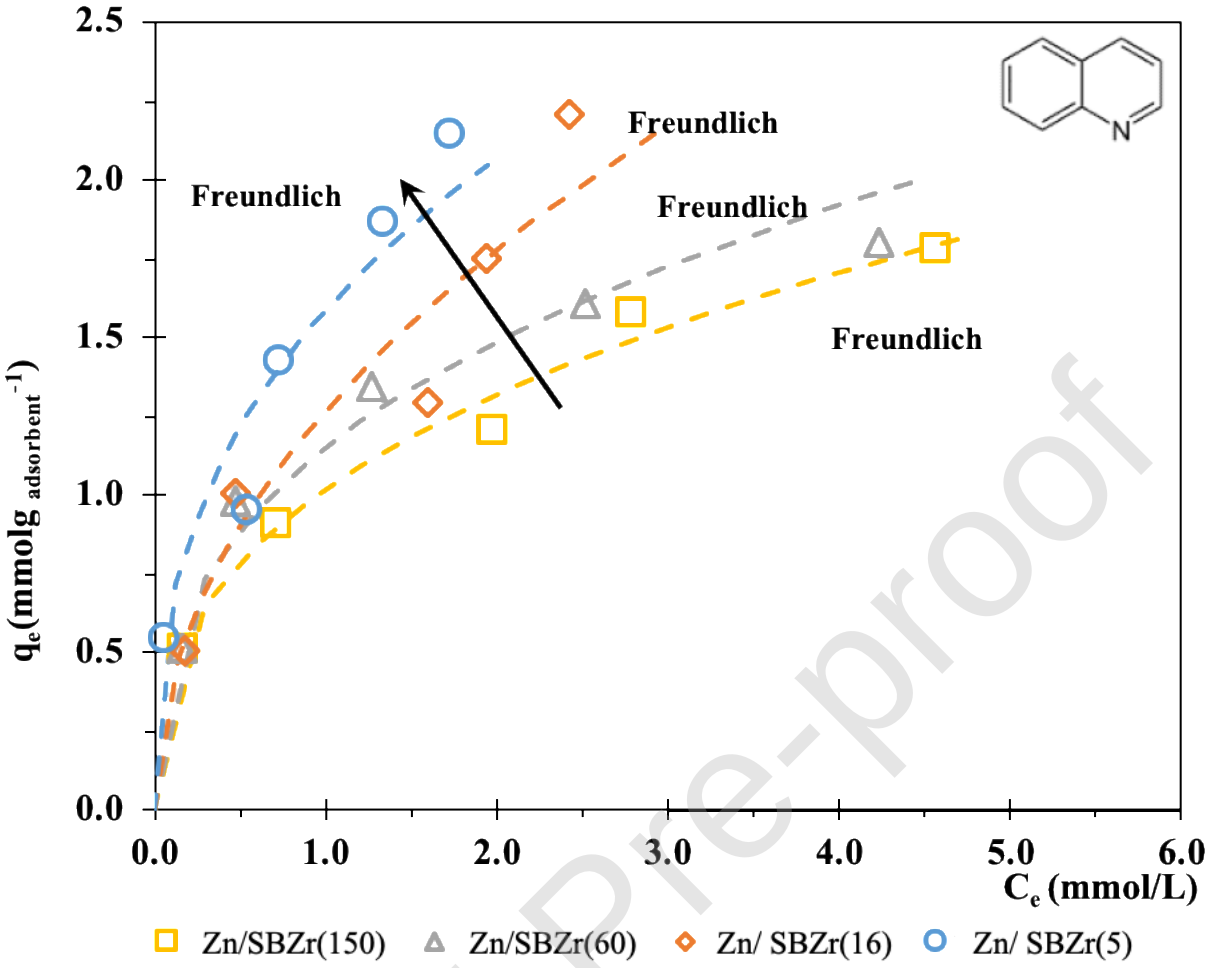

Figure 12. Adsorption isotherms of Q on Zn/SBZr(X). Fitted to experimental data in dashed lines.

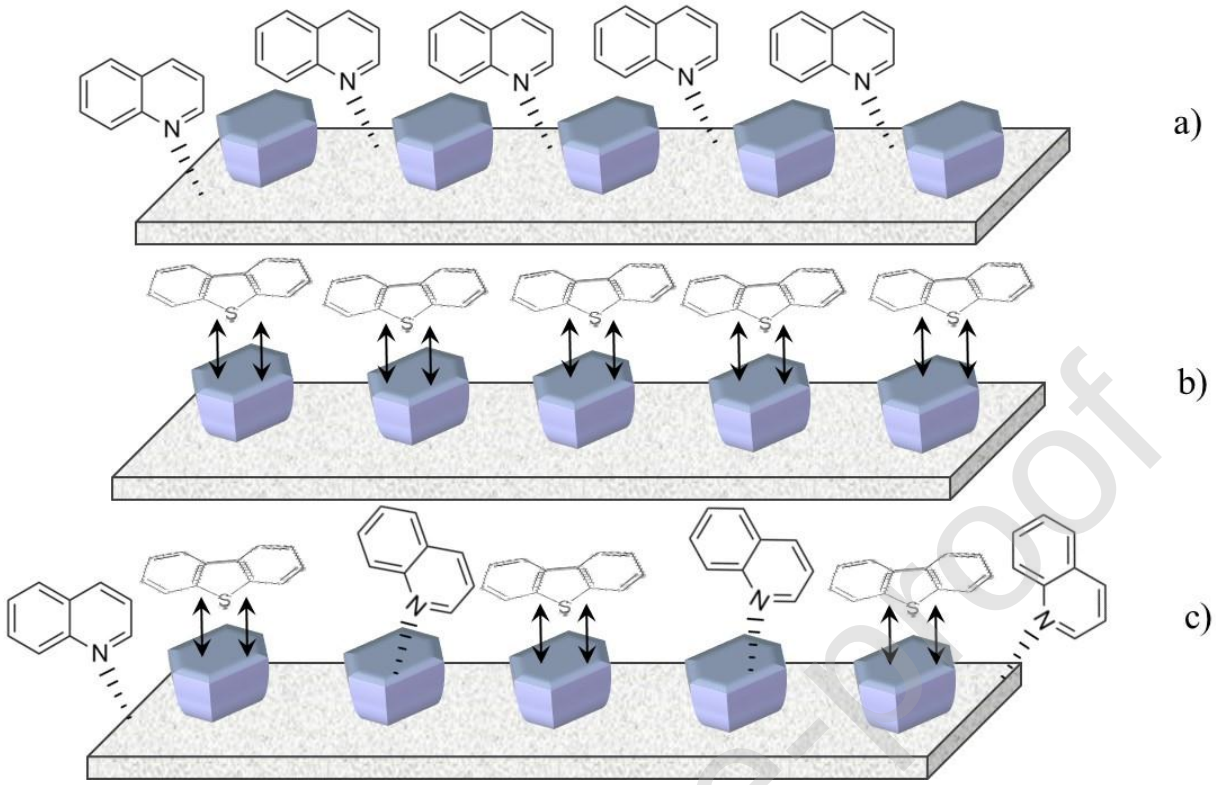

Figure 13. A model mechanism proposed to adsorption of Q and DBT on Zn/SiZr(X) adsorbents.

Table 1. Results of nitrogen physisorption for materials SBA-15 at several Si/Zr ratio.

Material	S_{BET} (m^2g^{-1})	V_p (cm^3g^{-1})	d_p (nm)	d_{100} (nm)	a_0 (nm)	E_p (nm)
SBA	665	1.02	5.7	11.2	12.9	7.2
SBZr(5)	554	0.78	5.6	10.8	12.4	6.8
SBZr(16)	553	0.84	5.8	11.0	12.8	7.0
SBZr(60)	730	1.05	5.9	11.3	13.1	7.1
SBZr(150)	758	1.11	5.9	11.2	12.9	7.0
Zn/SBZr(5)	478	0.71	5.5	10.5	12.1	6.6

S_{BET}= superface area, V_p = pore volume, d_p= pore diameter, d_{100}= interplanar distance, a_0= unit cell parameter ($a_0=2\,d_{100}/\sqrt{3}$), E_p= wall thickness ($E_p= a_0- d_p$).

Table 2. Elementary chemical analysis: EDXS

ELEMENT	Zn/SBZr(5)		Zn/SBZr(16)		Zn/SBZr(60)		Zn/SBZr(150)	
LINE	***wt. %***	***at.%***	***wt. %***	***at.%***	***wt. %***	***at.%***	***wt. %***	***at.%***
O K	47.78	65.60	47.07	64.92	51.73	66.04	50.32	64.95
Si K	39.75	31.09	40.33	31.70	45.70	33.25	46.23	34.00
Zn L	3.17	1.06	3.44	1.16	1.60	0.50	3.05	0.96
Zr L	9.29	2.24	9.16	2.21	0.97	0.22	0.40	0.09
Total	100	100	100	100	100	100	100	100

Table 3. Adsorption constants of Q and DBT* using SBA at several SBZr(X).

SBZr(X)	k_{ads} (g_{ads} $mmol^{-1}min^{-1}$)									
	50 ppm		100 ppm		150 ppm		200 ppm		250 ppm	
	Q	DBT	Q	DBT	Q	DBT	Q	DBT	Q	DBT
5	1.51	0.10	0.12	0.08	0.48	0.03	0.58	1.21	0.53	0.02
16	6.13	3.14	0.25	0.35	0.51	0.22	0.16	0.25	0.25	0.33
60	1.70	5.83	1.93	0.33	0.43	2.15	0.36	0.32	0.35	2.34
150	3.81	0.24	1.57	0.17	0.74	1.90	1.90	1.00	0.96	0.17

*[DBT] = 500 ppm

Table 4. The amount adsorbed by adsorbent gram (q_e) of Q and DBT* using SBZr(X).

SBZr(X)	q_e ($mmol^{-1}$ g_{ads}^{-1}) 50 ppm		100 ppm		150 ppm		200 ppm		250 ppm	
	Q	DBT	Q	DBT	Q	DBT	Q	DBT	Q	DBT
5	0.45	0.31	0.98	0.32	1.42	0.32	2.05	0.24	2.32	0.27
16	0.27	0.04	0.65	0.08	1.12	0.11	1.94	0.12	1.44	0.12
60	0.46	0.07	0.70	0.28	1.50	0.14	2.08	0.34	2.24	0.07
150	0.37	0.08	1.01	0.17	1.31	0.12	1.67	0.15	2.33	0.12

*[DBT] = 500 ppm

Table 5. The amount adsorbed by adsorbent gram (q_e) of Q and DBT* using Zn/SBZr(X) at several SiZr(X) ratio.

Zn/SBZr(X)	q_e ($mmolg_{ads}^{-1}$) 50 ppm		100 ppm		150 ppm		200 ppm		250 ppm	
	Q	DBT	Q	DBT	Q	DBT	Q	DBT	Q	DBT
5	0.55	1.86	0.96	1.81	1.43	1.81	1.87	1.40	2.20	1.30
16	0.50	2.20	1.00	1.90	1.30	1.81	1.75	1.58	2.20	1.20
60	0.51	1.60	0.98	1.07	1.35	1.00	1.61	0.89	1.80	0.60
150	0.51	0.70	0.91	0.65	1.21	0.63	1.60	0.30	1.78	0.30

*[DBT] = 500 ppm

Table 6. Parameters of the Freundlich isotherm of the adsorbents of Zn/SBZr(X).

	Zn/SBZr(5)	Zn/SiZr(16)	Zn/SiZr(60)	Zn/SiZr(150)
K_F	1.60	1.27	1.15	1.02
1/n	0.39	0.49	0.37	0.37
R^2	0.96	0.94	0.96	0.99

Table 7. Regeneration results of Q (250 ppm) and DBT* employing Zn/SBZr(5).

Regeneration Number	q_e ($mmolg_{adsorbent}^{-1}$)		k_{ads} ($mmolg_{adsorbent}^{-1}$)		Removal (%)	
	Q	DBT	Q	DBT	Q	DBT
0	2.2	1.3	0.76	0.38	88.0	65.0
1	1.5	0.68	0.15	0.11	55.0	29.4
2	1.5	0.88	0.11	0.07	33.0	22.4
3	1.7	0.96	0.11	0.05	32.3	20.4

*[DBT] = 500 ppm